Science of the Total Environment 851 (2022) 158234

Contents lists available at ScienceDirect

Science of the Total Environment

journal homepage: www.elsevier.com/locate/scitotenv

Integration of reference data from different Rapid-E devices supports automatic pollen detection in more locations

Predrag Matavulj [a,*], Antonella Cristofori [b], Fabiana Cristofolini [b], Elena Gottardini [b], Sanja Brdar [a], Branko Sikoparija [a]

[a] BioSense Institute – Research Institute for Information Technologies in Biosystems, University of Novi Sad, Dr Zorana Djindjica 1, 21000 Novi Sad, Serbia
[b] Research and Innovation Centre - Fondazione Edmund Mach, Via E. Mach, 1, 38010 San Michele all'Adige, Italy

HIGHLIGHTS

- Models trained on reference data from one device lose performance on another device.
- Variability of signals is higher between devices than among pollen taxa.
- The domain adaptation method improves correlation with Hirst data.
- Mixed models built on two reference datasets improve pollen classification.

GRAPHICAL ABSTRACT

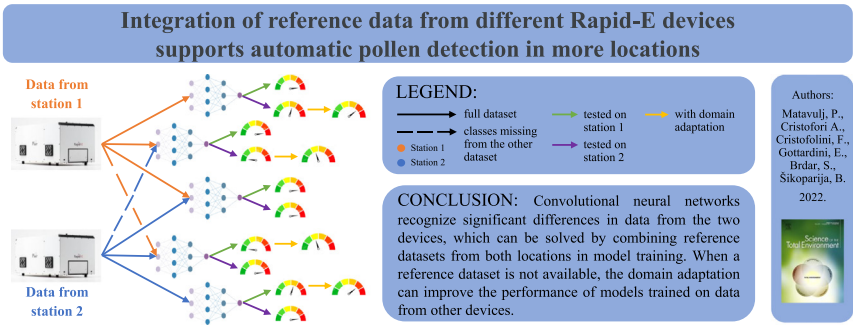

ARTICLE INFO

Editor: Pavlos Kassomenos

Keywords:
Aerobiology
Airborne pollen
Fluorescence
Classification
Machine learning
Domain adaptation

ABSTRACT

Pollen is the most common cause of seasonal allergies, affecting over 33 % of the European population, even when considering only grasses. Informing the population and clinicians in real-time about the actual presence of pollen in the atmosphere is essential to reduce its harmful health and economic impact. Thus, there is a growing network of automatic particle analysers, and the reproducibility and transferability of implemented models are recommended since a reference dataset for local pollen of interest needs to be collected for each device to classify pollen, which is complex and time-consuming. Therefore, it would be beneficial to incorporate the reference dataset collected from other devices in different locations. However, it must be considered that laser-induced data are prone to device-specific noise due to laser and detector sensibility. This study collected data from two Rapid-E bioaerosol identifiers in Serbia and Italy and implemented a multi-modal convolutional neural network for pollen classification. We showed that models lost their performance when trained on data from one and tested on another device, not only in terms of the recognition ability but also in comparison with the manual measurements from Hirst-type traps. To enable pollen classification with just one model in both study locations, we first included the missing pollen classes in the dataset from the other study location, but it showed poor results, implying that data of one pollen class from different devices are more different than data of different pollen classes from one device. Combining all available reference data in a single model enabled the classification of a higher number of pollen classes in both study locations. Finally, we implemented a domain adaptation method, which improved the recognition ability and the correlations of transferred models only for several pollen classes.

* Corresponding author.
E-mail address: matavulj.predrag@biosense.rs (P. Matavulj).

http://dx.doi.org/10.1016/j.scitotenv.2022.158234
Received 14 June 2022; Received in revised form 12 August 2022; Accepted 19 August 2022
Available online 23 August 2022

1. Introduction

Pollen monitoring has a long history, based on the pioneer experimental research of Blackley, back in the 1870s, on the aetiology of hay fever in England, where pollen was defined as the cause of allergic diseases (Blackley, 1873). During these studies, the first rudimentary suction and passive samplers were designed to search for quali-quantitative evidence connecting the hay fever symptoms to airborne pollen.

Nowadays, the burden of allergies worldwide is significant and constantly increasing due to urbanization, air pollution, and climate change (Barnes, 2018, D'Amato et al., 2015). In the USA, allergic rhinitis affects 24.4 million people, with children representing >20 % of the morbid population (Centers for Disease Control and Prevention, 2018; American College of Allergy, Asthma, and Immunology, 2018); the standardized sensitization rate to pollen for the European population is over 33 %, even when considering only grasses (Burbach et al., 2009). Vulnerable groups, such as children, are mostly impacted by pollen. The prevalence of rhinoconjunctivitis in 13–14-year-olds reaches 14.6 % worldwide (Ait-Khaled et al., 2009), with a sevenfold increased risk of asthma in the preadolescent period when severe attacks of allergic rhinitis occur (Barr et al., 2014).

The extent and efficacy of the treatment of the allergic disease are demonstrated to be highly related to the actual pollen exposure (de Weger et al., 2013; de Weger et al., 2021; Durham et al., 2014), especially in the early pollen season, when symptom severity is strictly related to the airborne pollen load (Sakurai et al., 2018). Informing the population and clinicians about the actual presence of pollen in the atmosphere is therefore essential and supported by the many pollen monitoring stations worldwide, primarily detailed in an interactive map developed by Buters et al. (2018). The vast majority of countries collect airborne pollen with volumetric Hirst-type traps, working on the basic principle of the rudimentary Blackley's suction sampler (Blackley, 1873), where airborne pollen impacts an adhesive surface and a manual optical analysis of pollen grains is performed by light microscopy: EN 16868:2019 (CEN, 2019). Since the procedure is time-consuming and requires a high level of personnel training, much research is focused on finding alternative approaches to optimize the timing and quality of pollen analysis, starting from spectroscopy to DNA based research (Gottardini et al., 2007; Johnson et al., 2021; Laucks and Davis, 1998; Leontidou et al., 2021; Longhi et al., 2009).

First attempts of the application of image analysis techniques were developed in the late 1990s, based on the evaluation of specific morphological features of the single fungal spore (Benyon et al., 1999) or pollen grain (Li and Flenley, 1999), analysed by different statistical methods (discrimination analysis, neural networks). The optical analysis is the most promising for airborne pollen monitoring because, even if the precision of the identification is best achievable via molecular techniques (Polling et al., 2022), the quantification of pollen load is performed better (Geller-Bernstein and Portnoy, 2019).

A new era is starting for airborne pollen monitoring, with the fast development of different optical devices capable of real-time or near real-time automatic sample collection, analysis, and data processing. Two main basic principles are exploited: i) automatic image analysis-based pollen count, with particles collected on tape or slide, and a differed (Boucher et al., 2002) or near real-time analysis (Oteros et al., 2015); ii) flow cytometers suctioning the airborne particles, analysing automatically in real-time the morphological and/or fluorescence parameters of pollen grains (Mitsumoto et al., 2010; Sauvageat et al., 2020). Up to 2018, only 1 % of pollen samplers were automatic worldwide (8 out of 525 in Europe; Buters et al., 2018), except in Japanese "Hanakosan" in which the majority of analysers are automatic, based on the Yamatronics KH-3000 technology (Buters et al., 2022). Therefore, great research for the development of automatic particle analysers and the reproducibility of implemented models is needed. This is of utter importance when having in mind that there are a number of models developed for forecasting allergenic airborne pollen, both receptor-oriented (Scheifinger et al., 2013) and source-oriented (Sofiev et al., 2013), that could benefit from assimilation with real-time measurements (Sofiev, 2019).

The Rapid-E real-time bioaerosol detector (Plair SA) works on the analysis of a combination of the scattered light patterns and fluorescence spectroscopy, representing particle morphological and chemical properties (Sauliene et al., 2019). The best performance in pollen classification can be obtained by entering Rapid-E data in a multimodal convolutional neural network, i.e., a network that takes multiple inputs simultaneously and outputs a prediction (Sauliene et al., 2019). The convolutional network output on Rapid-E data is tested against the standard sampling and analysis following EN 16868:2019. The results indicated that 14 out of 22 pollen classes have a strong positive relationship with >0.5 correlation (Cohen, 1988; Tesendic et al., 2020).

To classify pollen at one station, a reference dataset must be collected, which is complex and time-consuming (Tesendic et al., 2020). To be included in the reference dataset, calibration is performed by collecting single-taxa reference pollen samples from plants and exposing them to the device in a controlled environment (Sauliene et al., 2019). Therefore, it would be beneficial to incorporate in the analysis reference datasets collected from other devices in different locations.

However, laser-induced data are prone to device-specific noise due to laser and detector sensibility (Huffman et al., 2019; Konemann et al., 2019; Robinson et al., 2017), which is critical when transferring a model trained on data from one device to the other. The model can lose between 13 and 26 % of recognition ability when trained on a reference dataset from one Rapid-E device and tested on a reference dataset from another Rapid-E device, even when the reference pollen samples used for the calibration are the same for both devices (Matavulj et al., 2021); this implies the need for the inter-calibration of instruments, as with some other devices, e.g., BAA500 (Plaza et al., 2022). Furthermore, Matavulj et al. (2021) did not include the comparison of the Rapid-E signals with the standard EN 16868:2019, which would be an important step further since fresh pollen used as reference material for calibration may not ideally represent pollen suspended in the air (Tesendic et al., 2020).

This study collected data from two devices, one located in Novi Sad, Serbia, and the other in San Michele all'Adige, Italy. The reference pollen samples are different for the two devices. The end goal is to classify pollen as best as possible in both study locations, with minimum preparations and costs. Ideally, this implies that we can employ a model trained on reference datasets from different devices in any other location. First, we will show how the model performance changes when the models are trained on a dataset from one device and tested on a dataset from another when the reference pollen samples are different for the two devices. Afterward, we will evaluate our model performance in correctly identifying pollen in the air by comparing it with the standard EN 16868:2019. Furthermore, since the two study locations have different pollen taxa in the air, to enable pollen classification with just one model in both study locations, we will test the combinations of the reference datasets, first by including just the missing classes in the dataset from the other study location, and then by mixing all available datasets. Finally, we will implement a domain adaptation method (Ganin and Lempitsky, 2015), which improves the performance of models transferred from a Rapid-E device to the other by 13 % (Matavulj et al., 2021) and test the method against the standard EN 16868:2019.

2. Material and methods

2.1. Study location

The study was conducted in San Michele all'Adige, Italy (Latitude 46.19°N, Longitude 11.13°E) and Novi Sad, Serbia (Latitude 45.25°N, Longitude 19.85°E) (Fig. 1), included in the Alpine and Pannonian biogeographical region, respectively.

San Michele all'Adige is located on the Adige valley floor (Trentino-Alto Adige region, Northern Italy), 220 m above sea level, in a rural area mainly cultivated at vineyards and apple orchards. The lateral slopes are dominated by mixed forests, including *Pinus sylvestris*, *Ostrya carpinifolia*,

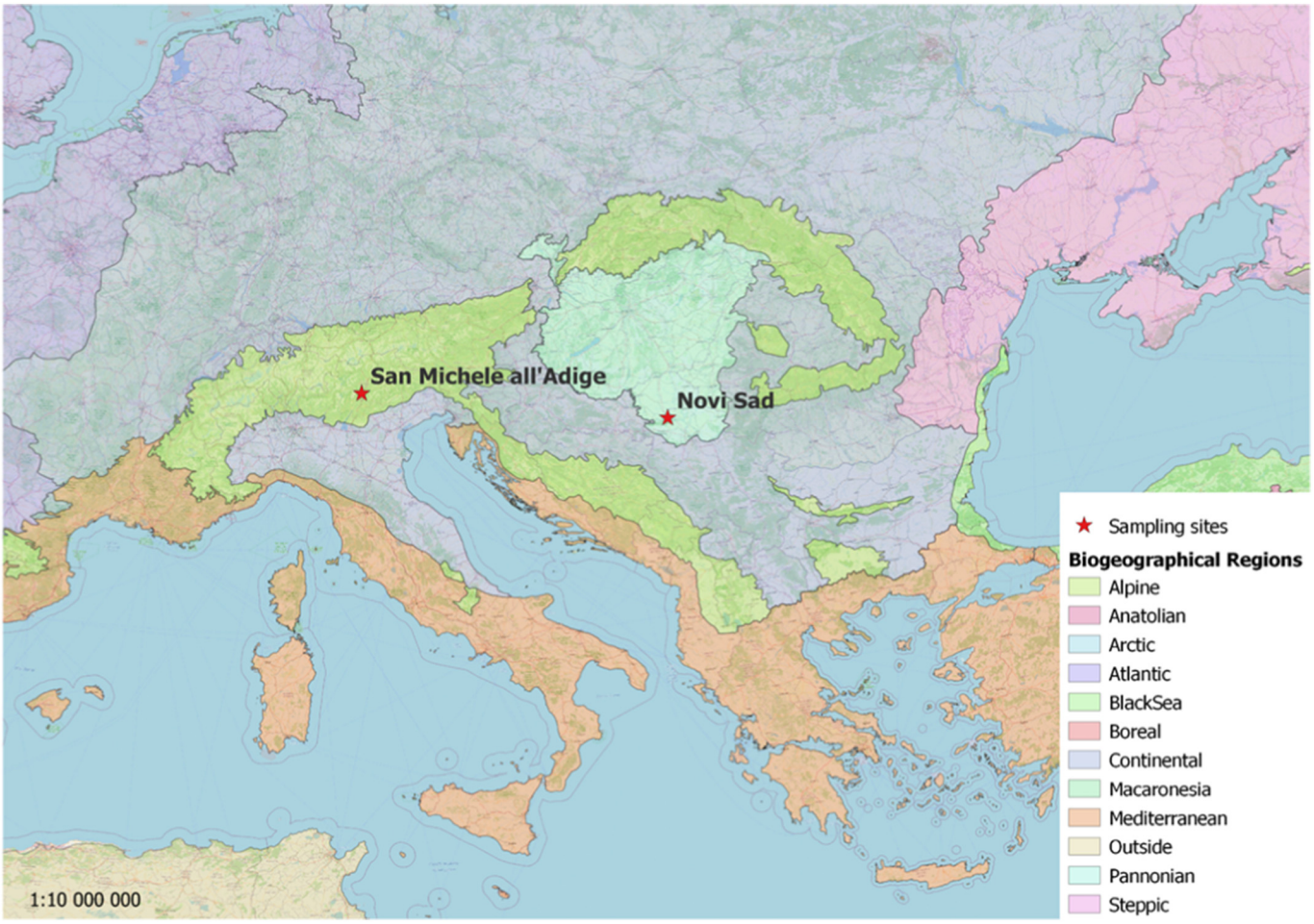

Fig. 1. Map of the Biogeographical regions (2016 update), with the location of the aerobiological stations (red stars) equipped with the PLAIR Rapid-E devices, which data are included in the present paper. The biogeographical regions dataset contains the official delineations used in the Habitats Directive (92/43/EEC) and for the EMERALD Network set up under the Convention on the Conservation of European Wildlife and Natural Habitats (Bern Convention) (European Environment Agency, 2016).

Fraxinus ornus, *Quercus pubescens*, coniferous forests dominated by *Pinus sylvestris*, *P. nigra*, and *Picea excelsa*, and broad-leaved forests of *Fagus sylvatica*, *Fraxinus ornus*, *Ostrya carpinifolia*, *Quercus pubescens* (Leontidou et al., 2018). The climate is oceanic-temperate, with a mean annual temperature of 11–14 °C and annual precipitation between 700 and 1600 mm.

Novi Sad is situated in the southern part of the Pannonian plain (Serbia) at 80 m above sea level. The region is dominated by arable crop production that creates habitats for numerous anemophilous ruderal/weed plants, i.e., *Ambrosia* sp. *Artemisia* sp., Cannabaceae. The location of the aerobiological station is close to Fruska Gora mountain, where mixed mesophilous forests with associations of *Tilia* sp., *Quercus* sp., *Carpinus betulus*, and *Fagus sylvatica* are distributed. There are also numerous stands of *Fraxinus* sp., *Corylus* sp., *Alnus* sp., *Morus* sp., *Juglans* sp. In addition to the region's natural vegetation, the city of Novi Sad is rich in a variety of ornamental and urban vegetation (i.e., *Platanus acerifolia*, *Acer negundo*, *Broussonetia papirifera*) that contribute to the spectra of pollen suspended in the atmosphere.

2.2. Airborne pollen measurements

The aerobiological samples are collected and analysed using the Rapid-E bioaerosol monitor designed and produced by Plair SA. To validate the performance of the automatic measurements, standard measurements EN 16868:2019 (CEN, 2019) are performed simultaneously in close vicinity by using the standard Hirst (1952) type volumetric samplers commonly adopted for airborne pollen monitoring in Europe and many other parts of the world (Buters et al., 2018). The study period extends from 18 July 2018 to 12 July 2019.

2.2.1. Standard volumetric measurements

Standard Hirst type volumetric measurements (EN 16868:2019) are performed using Lanzoni VPPS2000 devices with a continuous inlet airflow of 10 l min^{-1}, through an orifice oriented towards the direction of the wind. The particles suspended in the atmosphere are impacted onto an adhesive tape mounted on a drum that rotates at 2 mm per hour behind the 2 mm × 14 mm orifice. A 48 mm section of tape corresponding to a 24 h sample is mounted on a microscope slide and analysed under a light microscope at an ×400 magnification.

To obtain pollen concentrations from samples in Novi Sad, the daily samples (00–24 h CET) were scanned at three horizontal transects corresponding to 11.57 % of the total sample, and pollen grains were detected and counted. In San Michele all'Adige, the daily samples (00–24 h CET) were scanned at four horizontal transects corresponding to 14.28 % of the total sample, and pollen grains were detected and counted. Obtained data are converted to pollen concentrations expressed as the number of pollen grains per cubic meter of air (pollen m^{-3}) (Galan et al., 2017). The analysis of aerobiological samples as described is in line with the international standard EN 16868:2019 and, as such, has an acceptable coefficient of variation at the repeatability conditions of up to 10 % for pollen concentrations >300 pollen m^{-3}, up to 20 % for pollen concentrations between 30 and 300 pollen m^{-3}, and up to 30 % for pollen concentrations between 10 and 30 pollen m^{-3}.

2.2.2. Automatic measurements

The Rapid-E instrument designed and produced by Plair SA continuously samples 2.8 l min^{-1} of air through a fixed two-layered Sigma-2 inlet (VDI 2119 2013). Each sampled particle interacts with two laser light sources resulting in scattered light and two fluorescence patterns (Sauliene et al., 2019), which provide information about their morphology and chemical composition (Kiselev et al., 2013).

In Novi Sad, the Rapid-E is installed on the roof level (20 m a.g.l.) in the vicinity of the Hirst-type pollen sampler (Fig. 2A). In San Michele all'Adige, the Rapid-E is located on the ground level, thus sampling at 2 m a.g.l., while the Hirst type pollen sampler is installed on a pole at 10 m a.g.l. For both Rapid-E devices, detections in the "smart pollen mode" are used, which quantify the number of particles >8 μm in optical diameter (Sikoparija et al., 2019).

Due to laser and detector individual sensibility, scattering light images and fluorescence signals obtained from Rapid-E devices are prone to noise, which is unique to the device, and creates a shift in data distributions from different devices (Matavulj et al., 2021) (Supplementary Fig. 1). Matavulj et al. (2021) calibrated two devices with 8 pollen types using the same reference material. They showed that the performances of models trained on a reference dataset from one device and tested on a reference dataset from another device dropped by 13–25 %.

Artificial intelligence is applied to obtain pollen concentrations from Rapid-E detections (Sauliene et al., 2019; Tesendic et al., 2020). The classifier architecture is based on a multi-modal convolutional neural network (CNN). Features are extracted for scattered light, fluorescence spectrum, and lifetime separately by convolutional and pooling layers, equalized in size, concatenated, and classified with a fully connected network and a log-softmax function (de Brebisson and Vincent, 2015). The CNN is trained with a negative log-likelihood error, and data batches are created manually to represent all classes equally, having 20 samples per class. Training optimization is performed with the Stochastic Gradient Descent algorithm with a 0.001 learning rate and a momentum of 0.9. Since the F1 score of a model trained with a higher learning rate oscillates more than that of a model with a lower learning rate (Matavulj et al., 2021), the learning rate is decreased to 0.00001 for the last 500 batches when the validation error flattens (when the last 1000 validation errors are greater than the minimum error). The models are evaluated with the weighted F1 score (Dice similarity coefficient, the Sorensen-Dice index), which calculates the F1 score for each class and finds their average weighted by the number of instances for each class. The F1 score is defined as the harmonic mean of the precision and recall: $F1 = 2 * \frac{precision * recall}{precision + recall}$, where precision measures the model's ability to classify a sample as the correct class, and recall measures how many samples classified as one class are correct.

Additionally, because of the shifts in data distributions from different devices, networks utilizing the domain adaptation technique (Ganin and Lempitsky, 2015) are trained, improving the classification accuracy by ~11 % when trained on a reference dataset from one Rapid-E device and tested on a dataset from another Rapid-E device (Matavulj et al., 2021). A fully connected network, representing a domain classifier, is trained in parallel with the class label classifier in a way not to learn the differences between two or more domains representing Rapid-E devices. This is achieved by utilizing a gradient-reversal layer (GRL) between the feature extractor and the domain classifier. GRL acts as an identity when the network processes data. So, in the traditional settings, this neural network would learn the differences between the devices. However, when calculating gradients to optimize the network, i.e., to learn, gradients are multiplied by a factor -λ, reversing them. As a result, the optimization is performed in the direction of the gradient, leading to a local maximum. Therefore, applying GRL enforces that this neural network does not learn the differences between the domains. For adapting domains, additional data is imputed in the network with labels representing different devices that generated the data.

To enable automatic detections of the most dominant airborne pollen, reference data from both Rapid-E devices are collected following the injection of known pollen in the device airflow. Since for most pollen types recorded in the atmosphere morphological analysis allows identification up to the level of genus, the automatic measurements aimed to identify pollen taxa, hereafter named "classes" (not referred to the taxonomical rank), represented in the training set by pollen from one or more plant taxa (Supplementary Table 1). In Novi Sad, pollen was kept in Petri dishes at room temperature before being injected into the sample airflow, as described by Sauliene et al. (2019). In San Michele all'Adige, pollen collected from plants was either used immediately after flower extraction or dried in a desiccator at 4 °C for 24 h and stored at 4 °C. Before injecting into the

Fig. 2. Setup of the simultaneous measurements using standard Hirst type device and automatic pollen Rapid-E device in (A) Novi Sad and (B) San Michele all'Adige.

airflow, stored pollen was rehydrated in a humid chamber for 2–4 h to ensure that a potential excessive loss of hydration is recovered. Reference pollen was injected by blowing particles with compressed air through a sterilized glass pipette into the sampling head, while isolated from the ambient air circulation by a temporary chamber surrounding the sampling head itself (Sauliene et al., 2019). In addition to the pollen of interest, the models are trained for a class named 'other aerosols', corresponding to measurements when no pollen is recorded in the atmosphere (as indicated by simultaneous measurements using the standard EN 16868:2019 method). It is critical to obtain a reference dataset that represents the variability of pollen present in the air, and that is robust enough to encompass the variability of signals between devices.

Rapid-E devices recorded 343,523 reference pollen samples in Novi Sad and 541,773 in San Michele all'Adige, and the collected datasets are used for training AI classification algorithms. The particles with signals of insufficient quality are filtered out. To be included in the analysis, particles need to have a maximum spectrum intensity higher than 2500, a scattering image size lower than 450, a maximum lifetime index between 10 and 44, and four maximum spectrum indices between 3 and 10. After filtering, 95,155 particles are included in the reference dataset from Novi Sad and 179,624 particles from San Michele all'Adige. Data is further pre-processed by converting the fluorescence signals into images and normalizing them into the 0–1 range, centering the scattered light image and smoothing the signals. Detailed pre-processing steps are explained in Tesendic et al. (2020). The reference dataset is split into training, validation, and test datasets. The classification model is fitted to the training dataset, containing 80 % of the data. The validation and the test datasets include 10 % of data each. The former is used to validate model performance during training and the latter to test the best performing model on the validation set. Additionally, random data from both Rapid-E devices are collected to adapt the domains, containing 6622 particles from Novi Sad and 8601 particles from San Michele all'Adige after filtering and pre-processing.

2.3. Model definition for the experimental setup

The performance of classification models is dependent on the reference dataset used for model training. To test if the models are transferable from one device to the other and to assess how different combinations of training datasets influence the model performance, the following classification models are trained:

- **Base models**: trained on reference dataset from only one device
  - base_NS - model trained only on reference dataset from Novi Sad (NS data) (22 classes)
  - base_NS_DA - same dataset as for base_NS, trained with the domain adaptation
  - base_SMA - model trained only on reference dataset from San Michele all'Adige (SMA data) (20 classes)
  - base_SMA_DA - same dataset as for base_SMA, trained with the domain adaptation
- **Partially mixed models**: along with a reference dataset from only one device, missing classes are added from the reference dataset of the other device, since the base models are missing some pollen taxa present in the air from the other study location.
  - partial_NS - model trained on NS dataset with the addition of Castanea, Olea, and Ostrya classes from San Michele all'Adige (25 classes)
  - partial_NS_DA - same dataset as for partial_NS, trained with the domain adaptation
  - partial_SMA - model trained on SMA dataset with the addition of Acer, Juglans, Moraceae, Platanus, and Tilia classes from Novi Sad (25 classes)
  - partial_SMA_DA - same dataset as for partial_SMA, trained with the domain adaptation
- **Fully mixed model**: classes that are present in both reference datasets are merged, while classes unique to one study location are utilized as they are
  - fully_mixed - trained with reference datasets from both study locations (25 classes)

2.4. Data analysis

The performance of the automatic detections is analysed by comparison to simultaneous, side-by-side, standard measurements (EN 16868:2019). Agreement between automatic and standard measurements is quantified by calculating correlation coefficients. The analysis is focused on days when average pollen concentrations measured by EN 16868:2019 exceeded ten pollen per cubic meter (m^{-3}), which is a threshold for calculating the uncertainty, referring to the standard EN 16868:2019. Limiting the analysis on concentrations >10 pollen m^{-3} excludes long zero tails and low values at the beginning and the end of the season, thus limiting the inflation of correlation coefficients and *p*-values due to seasonality. Initial data assessment using the Shapiro-Wilk test confirms that data do not follow a normal distribution, so the alternative non-parametric Spearman's correlation coefficients are calculated.

Besides the fact that each measured daily value of the standard EN 16868:2019 has a distinct uncertainty, we noticed that models trained on the same dataset have uncertainty too. We trained ten models with the same architecture and training set but with different weights to calculate the uncertainty of automatic pollen classifications. For each pollen class, we focus only on the part of the signal where the concentration of the EN 16868:2019 is higher than ten pollen m^{-3}. The obtained signal from each model is standardized to have zero mean and unit variance and subsequently mean and variance are calculated for each measurement (timestamp) over the ten signals.

To include the uncertainty in the analysis, we implemented the Monte Carlo-based perturbation method (Curran, 2015), which approximates the correlation coefficient distribution by creating N new data pairs ($N \geq 1000$ for statistical significance) representing Rapid-E and Hirst outputs and calculates the correlation for each of them. The correlation distributions follow the Gaussian distribution (Supplementary Fig. 1) and are therefore represented with mean and standard deviation.

3. Results

3.1. Tests on reference datasets

Confusion matrices for base models indicate that most pollen classes have a correct identification rate higher than 60 % when tested on a test dataset from the same device (Fig. 3A, Fig. 3B). The average F1 scores over the ten models are 55 % for base_SMA, 72.8 % for base_NS, and 62.9 % for fully_mixed. The average F1 score of the base_NS model is much higher than for the base_SMA model, while for the fully_mixed model, the F1 score has an in-between value. The performance deteriorates significantly when the base models are tested on the reference dataset from the other device. SMA data is classified as only a few pollen classes with the base_NS model, primarily as other (20 %), Moraceae (12 %), Acer (11 %), Ulmus (11 %), and Cannabaceae (8 %) (Fig. 3E). When the base_SMA is tested on NS data, the results are even worse, where 61 % of data is classified as other and 13 % as Corylus (Fig. 3C).

Models implementing domain adaptation improve the classifications of a reference dataset from the other device. Classifying NS data with the base_SMA_DA, only 11 % of data is classified as other, compared to 61 % with the base_SMA. We can see more evenly spread classifications, i.e., data is recognized with more classes, and the recognitions are improved (Fig. 3D). Although not as obvious, there is also an improvement for SMA data classified with the base_NS_DA (Fig. 3F). The five pollen classes that collected 62 % of data with the base_NS model now classify only 38 % of data with base_NS_DA.

Evaluating the partially_mixed models, the original classes show similar behavior to the base models, while the added classes work even better because there is no mixing between the classes from different devices. The model only confuses some pollen classes when analysed data come from the same device. Therefore, the F1 score is better for the partially_mixed models than the base models when tested on the dataset from the same

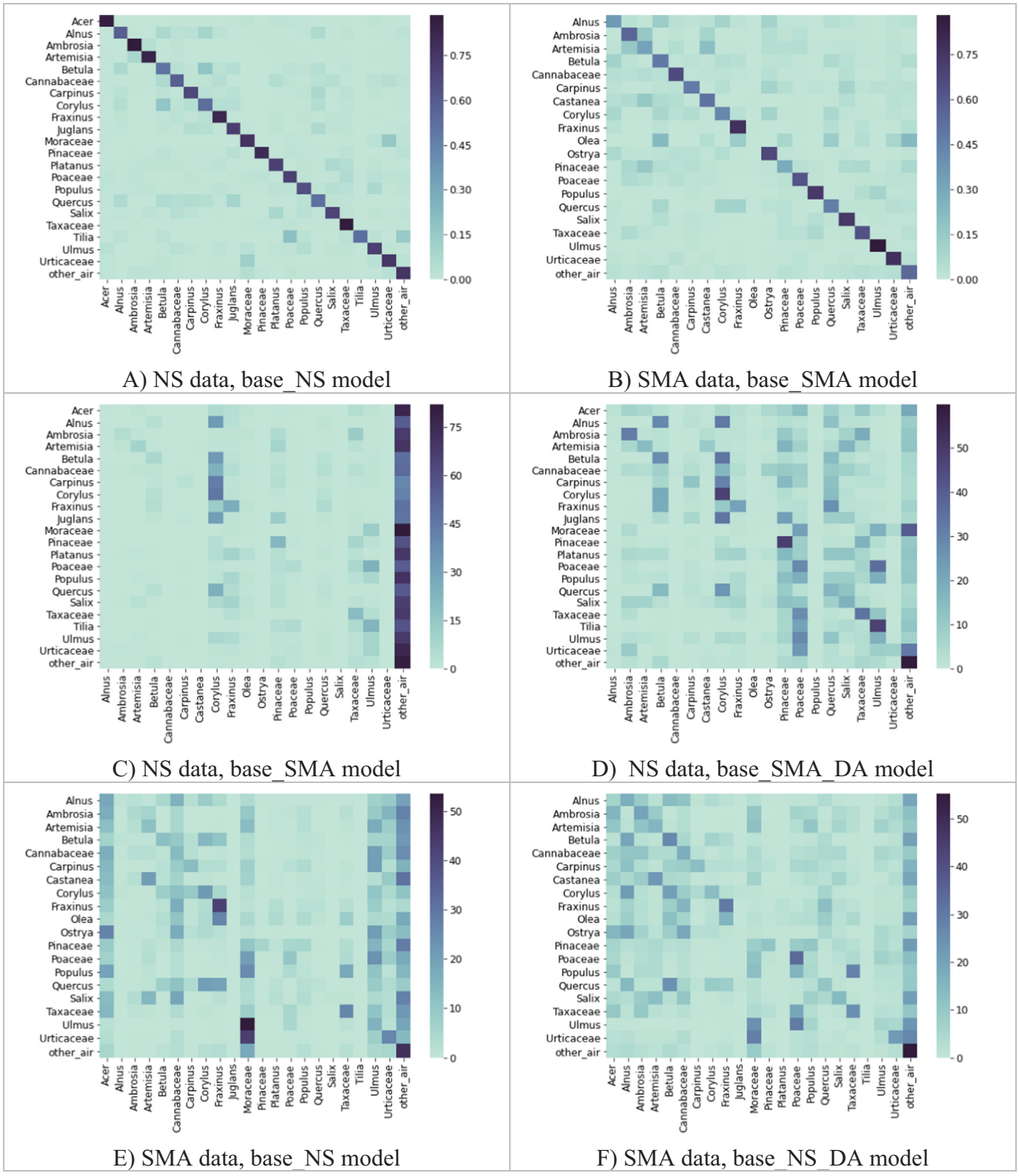

Fig. 3. Classification heatmaps, where on the y-axis is the data being classified, while on the x-axis are the model classes.

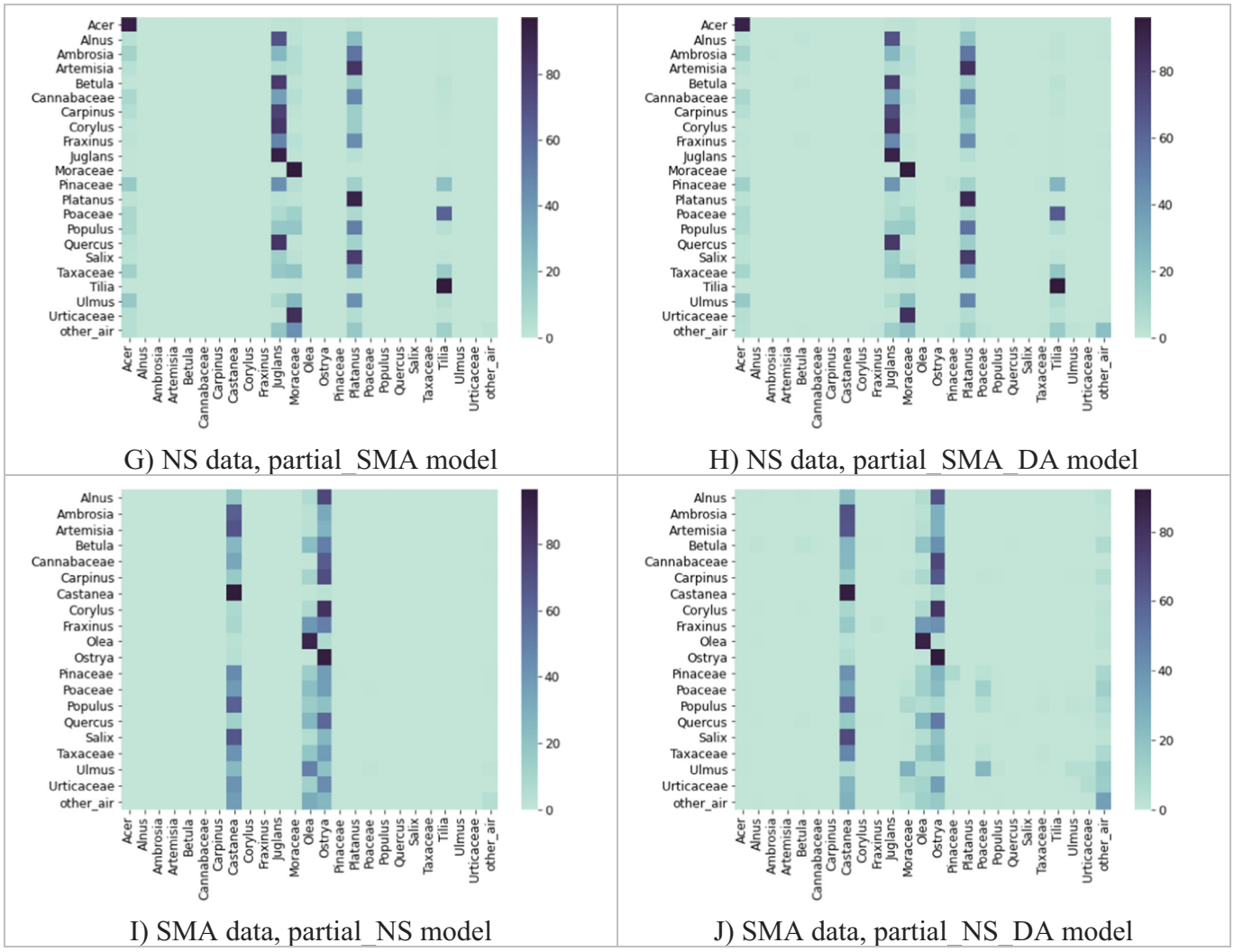

Fig. 3 (*continued*).

device. This is further noticed when tested on a dataset from the other device. No matter to which class they belong, all data are classified as the additional classes in the model (Fig. 3G, Fig. 3I).

Models implementing domain adaptation have slightly worse performance, around 3–5 %, when tested on a dataset from the same device because the model confuses data from the two devices. When tested on a dataset from the other device, there is a slight improvement, although barely noticeable (Fig. 3H, Fig. 3J).

3.2. Comparison of pollen classification signals obtained from automatic and conventional devices

First, we implemented the Monte Carlo-based perturbation method to include the uncertainty of Hirst and Rapid-E devices in the analysis. We created 10,000 data pairs of the Hirst and the Rapid-E signals for each pollen type and calculated their correlation. The results indicate that the correlation can be very stable even with the uncertainty included. E.g., for Ambrosia in Novi Sad, the mean correlation is 0.93 with a 0.0073 standard deviation (Supplementary Fig. 2). It should be noted that differences between the Rapid-E and the standard EN 16868:2019 (CEN, 2019) should be expected as they are also reported in previous studies with different devices (Buters et al., 2012; Molina et al., 2013). Furthermore, all mentions of correlation for a model refer to the mean of a correlation coefficient distribution between that model and the standard EN 16868:2019.

3.2.1. Base models

Since the base_NS model yielded the best F1 score, we employed it in both study locations (Fig. 4). The correlations, as expected, are weaker in San Michele all'Adige for most pollen classes except for Artemisia and Cannabaceae. The differences in correlation coefficients of the base_NS model in the two study locations are significant for almost all pollen classes. The most noticeable is 0.3 for Alnus, 0.67 for Artemisia, 0.62 for Cannabaceae, 0.38 for Quercus, and 0.54 for Salix. Otherwise, the differences are approximately 0.1–0.2. Therefore, we employed the base_SMA model for analysing the San Michele all'Adige pollen classes. The correlation coefficients are significantly improved compared to the base_NS model, except for Artemisia, Cannabaceae, and Corylus. For Betula and Pinaceae, correlation coefficients are also not improved. However, their correlation coefficients are not significant since they are <0.4. Finally, we applied the base_SMA model in Novi Sad, obtaining a drop in the performance for all types of pollen (Fig. 4). Furthermore, the uncertainty of a model trained on a dataset from one study location and applied to the other, measured by the standard deviation of the correlation coefficient distribution, is increased for all pollen classes included in the analysis in both study locations, except for Artemisia, Cannabaceae, and Corylus when base_NS model is applied in San Michele all'Adige.

We compared these models with the domain-adapted base models. Models applied to the study location where the training dataset originates perform similarly to the base models. However, when applied to the other

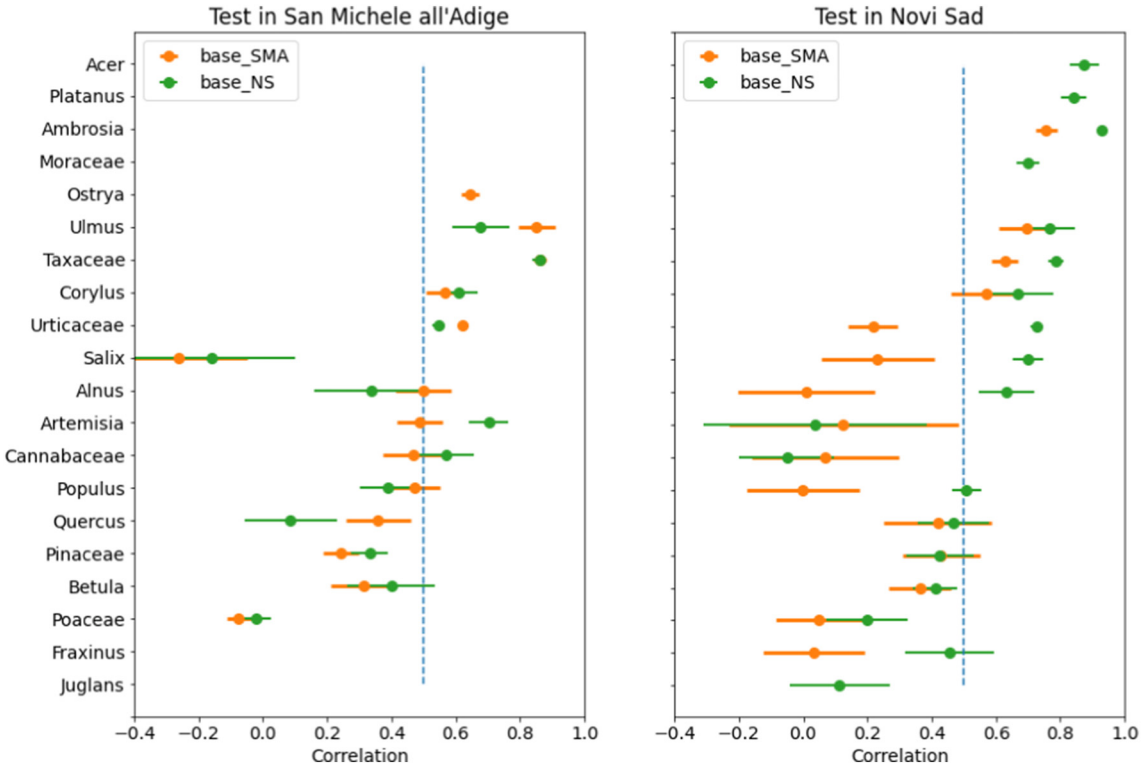

Fig. 4. Mean and standard deviation of Spearman's correlation coefficient distributions between automatic and standard EN 16868:2019 measurements of base models tested in both study locations. The right side of the dashed line at 0.5 indicates a strong positive relationship (Cohen, 1988).

study location, there are several improvements with the domain-adapted models. The difference for base_NS models employed in San Michele all'Adige is the correlation improvement of 0.23 for Alnus with the domain adaptation. The correlation distribution standard deviation (SD) decreases from 0.17 to 0.08, and the average *p*-value from the correlation calculation decreases from 0.27 to 0.03, making it more stable and meaningful. The average correlation is approximately the same for the rest of the pollen classes, except for Artemisia and Corylus, for which the correlation decreased by approximately 0.1. Furthermore, we noticed a drop in the average SD and *p*-values. For the base_SMA models in Novi Sad, the average correlation increased by 0.1, though the most meaningful improvement is 0.12 for Ambrosia and 0.39 for Salix. Correspondingly, the average SD decreased from 0.14 to 0.11, with the most noticeable drops for Ambrosia and Salix. A similar trend is with the p-values, where the average over all pollen classes dropped from 0.29 to 0.19.

3.2.2. Partially mixed models

Subsequently, we tested the partially_mixed models. The performance for these models is the same when tested in the study location from where the reference dataset originates. The model just ignores additional pollen classes. However, the performance deteriorates significantly when tested in the other study location. Almost all particles are classified as the classes obtained from the device in the other study location. Original classes are not working correctly, while classes from the other study location have good correlations compared to the base models, e.g., Acer and Moraceae have the same correlation while Platanus has a slightly reduced correlation, by 0.2. The other way around, Ostrya has a somewhat reduced correlation, by 0.1. Data from the standard EN 16868:2019 are not available for Castanea and Olea, which makes correlation calculation for those pollen classes not possible. Correspondingly, the measured standard deviation for the additional classes is like in the base models, and for the original reference dataset, the standard deviation increased significantly.

Implementing domain adaptation, we improved the correlation of the partial_NS model with the partial_NS_DA model in San Michele all'Adige from 0.09 to 0.25, while the SD dropped by 0.05. The most significant improvements are 0.5 for Alnus, 0.45 for Taxaceae, 0.5 for Ulmus, and 0.29 for Urticaceae. Furthermore, SD for these pollen classes dropped significantly, similarly to the *p*-values. Applying the partial_SMA_DA model in Novi Sad also improves the average correlation from 0.18 to 0. 27, with the most significant for Quercus from 0.1 to 0.4. There are a few more significant improvements in the correlation coefficients: 0.21 for Ambrosia, 0.22 for Betula, 0.35 for Corylus, 0.29 for Pinaceae, 0.29 for Salix, and 0.25 for Taxaceae. However, even the improved correlation coefficient does not exceed 0.4. Furthermore, the average SD dropped by 0.04.

3.2.3. Fully mixed model

Finally, we compared the fully_mixed model performance to the base models from the two study locations and observed that most pollen classes have a similar correlation coefficient for both models. The classes unique to one study location work as well as classes merged from the two devices, implying that when enough reference data are added from the two devices, the model is not influenced by the device-specific noise. The performance in San Michele all'Adige for Alnus, Populus, and Betula is enhanced, and for Urticaceae in Novi Sad, while the performance declined for Alnus in Novi Sad (Fig. 5).

3.2.4. Total pollen performance

The correlation coefficient of total pollen (sum of classified pollen classes) between the Rapid-E and the standard EN 16868:2019 in San Michele all'Adige is 0.45 for base_SMA, 0.44 for fully_mixed, and 0.42 for base_NS, improved with domain adaptation to 0.46 with base_NS_DA with 0.015 SD for all four models. In Novi Sad, the correlations are 0.85 for base_NS, 0.83 for fully_mixed, and 0.77 for base_SMA, also improved with domain adaptation to 0.8 with base_SM_DA with 0.007 SD for all models except base_SMA for which it is 0.01. Furthermore, correlations are improved with the domain adaptation for the partially_mixed models from 0.42 to 0.45 in San Michele all'Adige and from 0.66 to 0.73 in Novi Sad.

4. Discussion

4.1. Differences in data from different Rapid-E devices

The sensitivity of the devices yields data that seems to arise from different distributions, and the classification model trained on a reference dataset from one device loses its performance when tested on a reference dataset from the other device, even when the reference material used for the calibration of the devices is the same (Matavulj et al., 2021). Our data filtering relies heavily on positions of maximums: a maximum lifetime index must be between 10 and 44, and four maximum spectrum indices must be between 3 and 10, so the device-specific noise can impact the number of filtered particles. 67 % of particles are removed from SMA data, while from NS data, it is 75 %, which could be due to the shift in data distributions (Supplementary Fig. 1). However, local reference material, different for each study location, is used when calibrating the devices in this work. Therefore, different percentages of filtered particles could also result from different materials for the same pollen type. Furthermore, a high filtering percentage yields a much lower quantity of classified particles from the Rapid-E than the standard EN 16868:2019, which requires scaling factors to obtain the amount actually present (Tesendic et al., 2020). This presents a problem for classes which include pollen taxa already in low quantity in the air, and the classes with poor quality signals, e.g., low fluorescence intensity (Smith et al., 2022). Correlation coefficients are not reliable for those pollen classes. For that reason, Tilia and Carpinus are excluded from the analysis in Novi Sad, while Ambrosia, Carpinus, and Fraxinus are excluded from the analysis in San Michele all'Adige. At the same time, Artemisia in Novi Sad is presented in the results since the model yielded enough quantity to calculate the correlation. Still, only six days are available for the correlation calculation, and it is in low quantity in the air, which is expressed in the results.

4.2. Uncertainty analysis

We measured the uncertainty of the Rapid-E and Hirst devices based on the perturbation method (Curran, 2015) and included it in the analysis by working with the mean and SD of correlation coefficients. We showed that the models can exhibit stable correlation even with the uncertainty included, e.g., for Ambrosia in Novi Sad (Supplementary Fig. 2). The stability of the results expressed as the SD of the correlation coefficient distribution depends not only on the pollen type but on the location for which the correlation is calculated. Artemisia in Novi Sad, for example, has a very high SD of 0.35, while in San Michele all'Adige, SD is 0.07. We hypothesize that this is because *Artemisia* pollen quantity in Novi Sad is scarce. Furthermore, it is observed that pollen classes with higher correlation coefficients usually have smaller SD, although that is not always the case, e.g., for Poaceae in San Michele all'Adige (Fig. 5). One reason for this can be the number of particles in the air. There are many more Poaceae particles in San Michele all'Adige than, for example, Alnus or Populus, so they automatically have bigger uncertainty, which increases their SD. Of course, another reason for a larger SD can be the mixing of pollen classes too, so it is not strictly defined with the uncertainty.

4.3. Performance of base models

As a general result, there is a drop in performance when the models trained on data from one device are employed on the other, compared to the base model trained and tested on the same reference dataset. However, for some specific pollen classes, the model output data show unexpected results compared to standard data.

The results in San Michele all'Adige indicate a better correlation coefficient for Artemisia and Cannabaceae with the base_NS model than with the base_SMA model, which is not expected. Both Artemisia and Cannabaceae include different taxa in the two study locations (Supplementary Table 1)

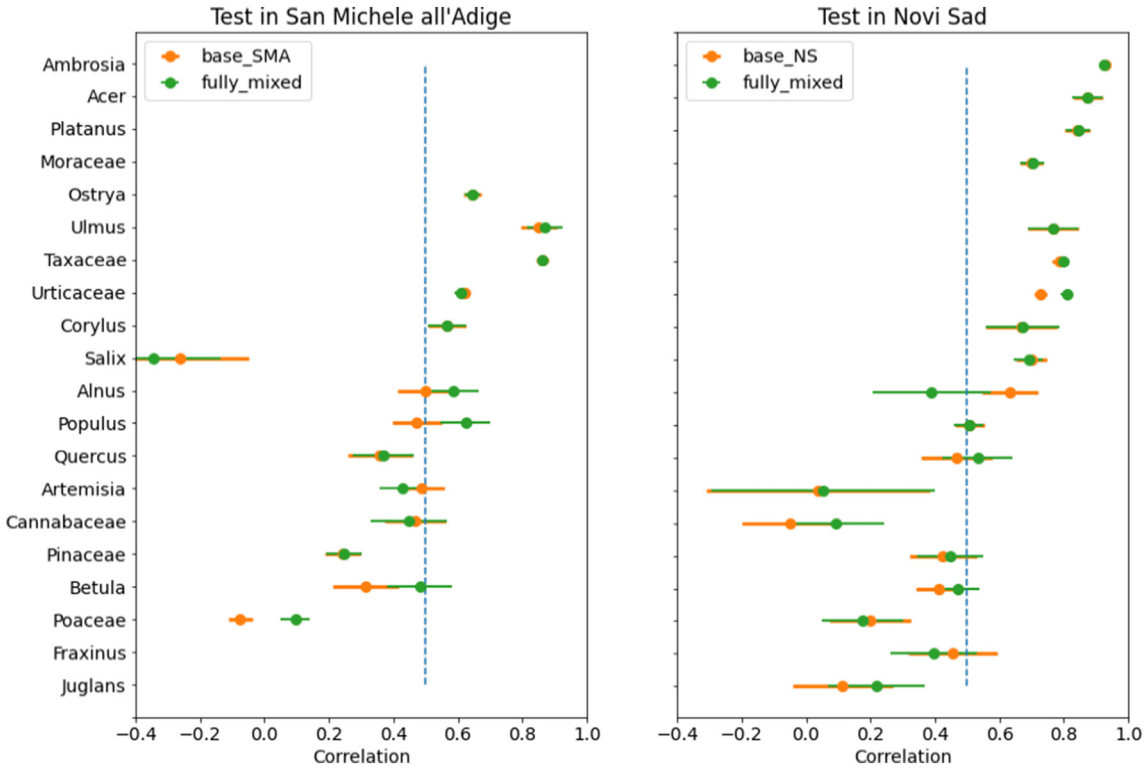

Fig. 5. Mean Spearman's correlation coefficients and its standard deviation, calculated between automatic and standard EN 16868:2019 measurements of base models and fully_mixed models tested in both study locations. The right side of the dashed line at 0.5 indicates a strong positive relationship (Cohen, 1988).

(Cristofori et al., 2020). We could argue that the representation in the NS data better matches pollen taxa suspended in the air in San Michele all'Adige for Artemisia and Cannabaceae. In San Michele all'Adige, training set for Cannabaceae class includes pollen from *Humulus lupulus*, which is a common plant, spontaneously growing in the region, while *Cannabis sativa* is rare and only cultivated (Aeschimann et al., 2004). Since hemp cultivation increased from 15,000 ha in 2013 to 40,000 ha in 2018 (Giupponi et al., 2020), we can conclude that training set for Cannabaceae in NS data better represents pollen in San Michele all'Adige since it contains *Cannabis sativa*, while SMA data does not. Correspondingly, the SD of correlation coefficient distributions for the two pollen classes is smaller with the base_NS model than with the base_SMA model.

4.4. Performance of partially mixed models

In the site-specific partially_mixed models, most training data derives from the reference dataset of the site itself, and only a few pollen classes derive from the reference dataset of the other study location. When applied to the other study location, the model classifies almost all measurements as the additional classes, with an extensive drop in the original class performance. This is expressed by the confusion matrices for these models. The reason for the low identification score of these models, when applied to the other study location, is the difference in detected fluorescence data between the two devices, which can be due to several reasons like the detector drift, laser sensitivity to temperature, the difference in excitation irradiance (Huffman et al., 2019). Matavulj et al. (2021) demonstrated that fluorescence spectrum data from two Rapid-E devices have big differences even when data are transformed with principal component analysis in two dimensions. Furthermore, Konemann et al. (2019) revealed that the measured irradiance of a new lamp could have ~200 % higher irradiance than a 3-year-old lamp, and Robinson et al. (2017) showed that detectors could be susceptible due to degradation or electronic gain, impacting light detection ability.

4.5. Mixing reference datasets from the two devices

When the reference dataset is available from both devices, we demonstrated that the fully_mixed model did not deteriorate pollen identification performance while enabling classifications of more pollen classes in both study locations. Alnus represents an exception because, while the performance with the fully_mixed model is improved when compared to the base model in San Michele all'Adige, it is worsened in Novi Sad. The reference datasets could explain this since populations of *Alnus glutinosa* dominate around Novi Sad and, together with *Alnus incana*, in San Michele all'Adige, and Alnus from NS data consists only of *Alnus glutinosa*, while SMA data uses three more additional taxa (Supplementary Table 1), with the highest number of particles of *Alnus viridis*, widespread in mountainous areas and barely present both in San Michele all'Adige and Novi Sad. Furthermore, the base_NS model works noticeably better for Artemisia and Cannabaceae than the fully_mixed model in San Michele all'Adige, which implies that the representation of the pollen taxa in the data used for model training is of great importance.

4.6. Domain adaptation

To make the model invariant to the device specifics in data without mixing the reference datasets from the two devices, we implemented the domain adaptation method from Ganin and Lempitsky (2015), which already showed improvements in the classification accuracy on Rapid-E data (Matavulj et al., 2021). However, the authors did not calculate correlation coefficients between the Rapid-E and the standard EN 16868:2019, which would be an important step further since fresh pollen used as reference material for calibration may not ideally represent pollen suspended in the air. Tesendic et al. (2020) showed that the model performance on the reference dataset can be misleading. They showed that, for example, the identification score for Betula is 88 % with a correlation coefficient of 0.17, while for Juglans, the identification score is 20 % but with a 0.85 correlation coefficient.

We showed that we can improve the model confusion matrices when testing the model on data from the other device by implementing the domain adaptation method from Ganin and Lempitsky (2015), although results are not as good as when training and testing it on data from the same device. Similarly, the correlations of the domain-adapted models built on the reference dataset from the other device are improved for some pollen classes, which is particularly useful when reference datasets from more devices are available. However, the improvement is not as good as with the models trained and tested on the same device. Therefore, other deep domain adaptation techniques, based on reconstruction, i.e., autoencoders (Ghifary et al., 2016; Glorot et al., 2011) or generative adversarial networks (Hoffman et al., 2017; Pei et al., 2018; Tzeng et al., 2015), should be investigated for further improvement of the results.

4.7. Performance of total pollen

The correlation between total pollen from real-time devices and Hirst-type samplers demonstrates the usability of the former to detect pollen, discriminating it from other bioaerosols. The correlation coefficients are stable with the uncertainty included, having SD in the range of 0.007 to 0.015. In San Michele all'Adige correlations are similar for all models with the values between 0.42 and 0.46, even for the partially_mixed_NS model, while in Novi Sad they go from 0.66 for the partially_mixed_SMA model to 0.85 for the base_NS model. The reason why the correlation of total pollen in San Michele all'Adige is much lower than in Novi Sad is unknown. One possible reason is that the Hirst sampler is 8 m above the Rapid-E in San Michele all'Adige. Furthermore, two other studies compared total pollen concentrations between the Rapid-E and the standard EN 16868:2019. One study obtained a correlation coefficient of 0.97 (Crouzy et al., 2016), and the other 0.41 (Tummon et al., 2021) with no indication of a reason for the difference.

4.8. Comparison with other studies

The only work involving the transferability of models between automated airborne particle identifiers is published in Oteros et al. (2020), who reported similar model performance at four different locations using the Hund-Wetzlar BAA500. However, there is little information about the model employed in the analysis since the model is fixed and integrated into the device. Furthermore, the BAA500 implements an image recognition-based method that is considerably less prone to noise than the fluorescence-based Rapid-E.

Regarding the correlation coefficients, the authors reported a positive correlation >0.5 for 10 out of 12 pollen classes. Furthermore, they obtained a strong positive correlation >0.8 for Alnus, Betula, and Poaceae, while our model cannot distinguish those classes very well. Sauvageat et al. (2020) successfully classified eight pollen classes on holographic images from the Swisens Poleno device. However, there are no published results for the comparison with manual measurements yet. Kawashima et al. (2017) reported a positive correlation >0.7 for just three out of six possible pollen classes using the Yamatronics KH-3000. However, the device's design quantifies particles in a predefined size range, so if there are different pollen classes whose sizes overlap, this will not distinguish them. Finally, O'Connor et al. (2014) reported a strong positive correlation with a Hirst-type trap for total pollen >0.9 for the waveband-integrated bioaerosol sensor (WIBS-4), which employs methods similar to Rapid-E. The authors did the experiments in two locations and obtained similar results. However, pollen concentrations were obtained applying thresholds on the size, shape, and fluorescence data obtained from the device, and no models were employed for the classification. Furthermore, another study with a newer device version (WIBS-NEO) reported a considerably lower correlation coefficient of 0.48 for total pollen (Tummon et al., 2021). No studies performed further pollen type classification.

The inherent choice of the laser wavelength applied on Rapid-E devices leads to challenges when identifying pollen types that emit low

fluorescence at 337 nm (Pohlker et al., 2013). This is the case with Alnus, Betula, Quercus, Juglans, Carpinus, and Corylus. Furthermore, unlike the image recognition-based methods, the high complexity of the Rapid-E signals makes it hard to check the data quality. Finally, the laser-induced signals from Rapid-E are much more prone to noise than the optical imagery. Thus, model transferability is a minor concern for devices utilizing optical microscopy.

5. Conclusion

This paper evaluates model transferability between two Rapid-E instruments, located in Novi Sad in the southern part of the Pannonian plain in Novi Sad, Serbia, and San Michele all'Adige, on the Adige valley floor in Northern Italy. The traditional Hirst-type pollen samplers, considered as a "golden standard" in pollen counting, were located in the vicinity of the Rapid-E in Novi Sad and 8 m above the Rapid-E in San Michele all'Adige to assess Rapid-E's signal quality. However, Hirst-type samplers have uncertainty, which we incorporated, along with the uncertainty of the models, in the correlation analysis by implementing the Monte Carlo-based perturbation method (Curran, 2015). The devices worked from 18 July 2018 to 12 July 2019.

The study results demonstrate a loss in performance of the classification models, represented by the F1 score, when a model trained on a reference dataset from one device is tested on a reference dataset from the other device. As a result, all data are classified in a few pollen classes. Similarly, models trained on a reference dataset that derives primarily from one location with only a few pollen classes originating from the reference dataset of the other study location, where the model is tested, classify all data as those few pollen classes, implying that data of the same pollen class from different devices are more diverse than data of different pollen classes from the same device. Implementation of the domain adaptation method, which attempts at adjusting the network weights to overlook the data differences from the two devices (Ganin and Lempitsky, 2015) improves the recognition rates of the transferred models, although not nearly as good as the original models.

Furthermore, we observed a deterioration of Spearman's correlation coefficients with the standard EN 16868:2019 of models trained on the reference dataset from one device are tested at the other study location. However, this is not true for Artemisia and Cannabaceae in San Michele all'Adige. For those classes, reference dataset from Novi Sad better describes airborne pollen in San Michelle all'Adige, implying that the choice of plant species that contribute to the pollen class for creating the reference dataset is important. The results are improved with the domain adaptation method for some pollen classes. But, similarly as with the F1 score, they are not as good as the original models. Therefore, other domain adaptation methods described in Subsection 4.6 should be investigated for better-quality performance. However, the described domain adaptation technique improves the average correlation coefficient and decreases the average SD, which is helpful if there is no or little available reference data from a device with no classification model. If the reference datasets from both devices are available, mixing them does not deteriorate pollen identification performance and enables classifications of more pollen taxa in both study locations. However, attention should be paid to which anemophilous plants are included in the mixed dataset to make it representative of the airborne pollen taxa in a certain area.

Although there is room for improvement, the results of this study show that the Rapid-E has the capability to detect most airborne pollen detected in the study area, and that the generalization power of a neural network model is increased by the integration of reference data from the two study sites, implying that the model is not influenced by the device-specific noise when enough reference data are mixed from the two devices. Furthermore, high correlation between automatic and Hirst-type measurement data opens the possibility for using real-time measurements data for assimilation with source-oriented dispersion models, improving their performance. Finally, the development of domain adaptation techniques in pollen classification could potentially replace the need for the intercalibration of the devices.

Supplementary data to this article can be found online at https://doi.org/10.1016/j.scitotenv.2022.158234.

Funding sources

We acknowledge support from COST Action CA18226 "New approaches in detection of pathogens and aeroallergens (ADOPT)" (www.cost.eu/actions/CA18226). This research was partially funded by the BREATHE project from the Science Fund of the Republic of Serbia PROMIS program, under grant agreement no. 6039613 and by the Ministry of Education, Science and Technological Development of the Republic of Serbia (grant agreement number 451-03-68/2022-14/200358). Measurement campaign in Novi Sad was supported by RealForAll project (2017HR-RS151) co-financed by the Interreg IPA Cross-border Cooperation program Croatia – Serbia 2014–2020 and Provincial secretariat for finances, Autonomous Province Vojvodina, Republic of Serbia (contract no. 102-401-337/2017-02-4-35-8). The sampling campaign in San Michele all'Adige was partially funded by PROJET II-JP 27.09.2017, co-financed by PLAIR S.A., and Banque Cantonale de Genève (BCGE).

Data availability

The data that has been used is confidential.

Declaration of competing interest

The authors declare that they have no known competing financial interests or personal relationships that could have appeared to influence the work reported in this paper.

References

Aeschimann, D., Lauber, K., Moser, D.M., Theurillat, J.-P., 2004. Flora alpina. Zanichelli, Bologna.

Ait-Khaled, N., Pearce, N., Anderson, H.R., Ellwood, P., Montefort, S., Shah, J., 2009. ISAAC Phase Three Study Group. Global map of the prevalence of symptoms of rhinoconjunctivitis in children: the International Study of Asthma and Allergies in Childhood (ISAAC) Phase Three. Allergy 64 (1), 123–148. https://doi.org/10.1111/j.1398-9995.2008.01884.x PMID: 19132975.

American College of Allergy, Asthma and Immunology, 2018. Allergy facts. http://acaai.org/news/facts-statistics/allergies. (Accessed 18 March 2022).

Barnes, C.S., 2018. Impact of climate change on pollen and respiratory disease. Curr Allergy Asthma Rep 18, 59. https://doi.org/10.1007/s11882-018-0813-7.

Barr, J.G., Al-Reefy, H., Fox, A.T., Hopkins, C., 2014. Allergic rhinitis in children. BMJ 349, 4153. https://doi.org/10.1136/bmj.g4153.

Benyon, F.H.L., Jones, A.S., Tovey, E.R., Stone, G., 1999. Differentiation of allergenic fungal spores by image analysis, with application to aerobiological counts. Aerobiologia 15, 211–223. https://doi.org/10.1023/A:1007501401024.

Blackley, C.H., 1873. Experimental Researches on the Causes and Nature of Catarrhus Æstivus. Bailierre, Tindall & Cox, King William Street, Strand, London.

Boucher, A., Hidalgo, P.J., Thonnat, M., Belmonte, J., Galan, C., Bonton, P., Tomczak, R., 2002. Development of a semi-automatic system for pollen recognition. Aerobiologia 18, 195–201. https://doi.org/10.1023/A:1021322813565.

Burbach, G.J., Heinzerling, L.M., Edenharter, G., Bachert, C., Bindslev-Jensen, C., Bonini, S., et al., 2009. GA(2)LEN skin test study II: clinical relevance of inhalant allergen sensitizations in Europe. Allergy 64, 1507–1515. https://doi.org/10.1111/j.1398-9995.2009.02089.x.

Buters, J., Thibaudon, M., Smith, M., Kennedy, R., Rantio-Lehtimaki, A., Albertini, R., et al., 2012. Release of bet v 1 from birch pollen from 5 European countries. Results from the HIALINE study. Atmos. Environ. 55, 496–505. https://doi.org/10.1016/j.atmosenv.2012.01.054.

Buters, J.T.M., Antunes, C., Galveias, A., Bergmann, K.C., Thibaudon, M., Galan, C., Schmidt-Weber, C., Oteros, J., 2018. Pollen and spore monitoring in the world. Clin. Transl. Allergy 8, 9. https://doi.org/10.1186/s13601-018-0197-8 PMID: 29636895; PMCID: PMC5883412.

Buters, J., Clot, B., Galán, C., Gehrig, R., Gilge, S., Hentges, F., et al., 2022. Automatic detection of airborne pollen: an overview. Aerobiologia. https://doi.org/10.1007/s10453-022-09750-x.

Centers for Disease Control and Prevention, 2018. 2018 National Health Interview Survey data. https://www.cdc.gov/climateandhealth/effects/allergen.htm. (Accessed 18 March 2022).

CEN, 2019. EN 16868:2019 (CEN, 2019) Ambient air - Sampling and analysis of airborne pollen grains and fungal spores for networks related to allergy - Volumetric Hirst method. CEN-CENELEC Management Centre: Rue de la Science 23, B-1040 Brussels, European Committee for Standardization. https://shop.austrian-standards.at/.

Cristofori, A., Bucher, E., Rossi, M., Cristofolini, F., Kofler, V., Prosser, F., Gottardini, E., 2020. The late flowering of invasive species contributes to the increase of Artemisia allergenic pollen in autumn: an analysis of 25 years of aerobiological data (1995–2019) in Trentino-Alto Adige (Northern Italy). Aerobiologia 36, 669–682. https://doi.org/10.1007/s10453-020-09663-7.

Cohen, J., 1988. Statistical Power Analysis for the Behavioral Sciences. New York, New York. https://doi.org/10.4324/9780203771587.

Crouzy, B., Stella, M., Konzelmann, T., Calpini, B., Clot, B., 2016. All-optical automatic pollen identification: towards an operational system. Atmos. Environ. 140, 202–212. https://doi.org/10.1016/j.atmosenv.2016.05.062.

Curran, P.A., 2015. Monte Carlo error analyses of spear-man's rank test. Instrumentation and Methods for Astrophysics. arXiv https://doi.org/10.48550/arXiv.1411.3816.

D'Amato, G., Holgate, S.T., Pawankar, R., Pawankar, R., Ledford, D.K., Cecchi, L., et al., 2015. Meteorological conditions, climate change, new emerging factors, and asthma and related allergic disorders. A statement of the world allergy organization. World Allergy Organ. J. 8, 1–52. https://doi.org/10.1186/s40413-015-0073-0.

de Brebisson, A., Vincent, P., 2015. An Exploration of Softmax Alternatives Belonging to the Spherical Loss Family. arXiv https://doi.org/10.48550/arxiv.1511.05042.

de Weger, L.A., Bergmann, K.C., Lehtimaki, A.R., Dahl, A., Buters, J., Dechamp, C., 2013. Impact of Pollen. Allergenic Pollen. Springer, Dordrecht. https://doi.org/10.1007/978-94-007-4881-1_6.

de Weger, L.A., van Hal, P.T.W., Bos, B., Molster, F., Mostert, M., Hiemstra, P.S., 2021. Personalized pollen monitoring and symptom scores: a feasibility study in grass pollen allergic patients. Front. Allergy 2, 628400. https://doi.org/10.3389/falgy.2021.628400.

Durham, S.R., Nelson, H.S., Nolte, H., Bernstein, D.I., Creticos, P.S., Li, Z., Andersen, J.S., 2014. Magnitude of efficacy measurements in grass allergy immunotherapy trials is highly dependent on pollen exposure. Allergy 69, 617–623. https://doi.org/10.1111/all.12373.

European Environment Agency, 2016. Biogeographical regions. http://www.eea.europa.eu/data-and-maps/data/biogeographical-regions-europe-3. (Accessed 3 November 2022).

Galan, C., Ariatti, A., Bonini, M., Clot, B., Crouzy, B., Dahl, A., et al., 2017. Recommended terminology for aerobiological studies. Aerobiologia 33 (3), 293–295. https://doi.org/10.1007/s10453-017-9496-0.

Ganin, Y., Lempitsky, V., 2015. Unsupervised domain adaptation by backpropagation. Proceedings of the 32nd International Conference on International Conference on Machine Learning (ICML'15). Volume 37, pp. 1180–1189. https://doi.org/10.48550/arXiv.1409.7495.

Geller-Bernstein, C., Portnoy, J.M., 2019. The clinical utility of pollen counts. Clin. Rev. Allergy Immunol. 57, 340–349. https://doi.org/10.1007/s12016-018-8698-8.

Ghifary, M., Kleijn, W.B., Zhang, M., Balduzzi, D., Li, W., 2016. Deep reconstruction classification networks for unsupervised domain adaptation. European Conference on Computer Vision. Springer, pp. 597–613 https://doi.org/10.48550/arXiv.1607.03516.

Giupponi, L., Leoni, V., Carrer, M., Ceciliani, G., Sala, S., Panseri, S., et al., 2020. Overview on Italian hemp production chain, related productive and commercial activities and legislative framework. Ital. J. Agron. https://doi.org/10.4081/ija.2020.1552.

Glorot, X., Bordes, A., Bengio, Y., 2011. Domain adaptation for large-scale sentiment classification: a deep learning approach. Proceedings of the 28th International Conference on Machine Learning (ICML'11). Omnipress, Madison, WI, USA, pp. 513–520. https://doi.org/10.5555/3104482.3104547.

Gottardini, E., Rossi, S., Cristofolini, F., Benedetti, L., 2007. Use of fourier transform infrared (FT-IR) spectroscopy as a tool for pollen identification. Aerobiologia 23, 211–219. https://doi.org/10.1007/s10453-007-9065-z.

Hirst, J.M., 1952. An automatic volumetric spore trap. Ann. Appl. Biol. 39, 257–265. https://doi.org/10.1111/j.1744-7348.1952.tb00904.x.

Hoffman, J., Tzeng, E., Park, T., Zhu, J., Isola, P., Saenko, K., 2017. Cycada: Cycle-consistent Adversarial Domain Adaptation. arXiv https://doi.org/10.48550/arXiv.1711.03213.

Huffman, A.J., Perring, A.E., Savage, N.J., Clot, B., Crouzy, B., Tummon, F., et al., 2019. Real-time sensing of bioaerosols: review and current perspectives. Aerosol Sci. Technol. 54 (5). https://doi.org/10.1080/02786826.2019.1664724.

Johnson, M.D., Fokar, M., Cox, R.D., Barnes, M.A., 2021. Airborne environmental DNA metabarcoding detects more diversity, with less sampling effort, than a traditional plant community survey. BMC Ecol. Evol. 21 (1), 218. https://doi.org/10.1186/s12862-021-01947-x PMID: 34872490; PMCID: PMC8647488.

Kawashima, S., Thibaudon, M., Matsuda, S., Fujita, T., Lemonis, N., Clot, B., Oliver, G., 2017. Automated pollen monitoring system using laser optics for observing seasonal changes in the concentration of total airborne pollen. Aerobiologia 33 (3), 351–362. https://doi.org/10.1007/s10453-017-9474-6.

Kiselev, D., Bonacina, L., Wolf, J.-P., 2013. A flash-lamp based device for fluorescence detection and identification of individual pollen grains. Rev. Sci. Instrum. 84, 033302. https://doi.org/10.1063/1.4793792.

Konemann, T., Savage, N., Klimach, T., Walter, D., Frohlich-Nowoisky, J., Su, 2019. Spectral Intensity Bioaerosol Sensor (SIBS): an instrument for spectrally resolved fluorescence detection of single particles in real time. Atmos. Meas. Tech. 12, 1337–1363. https://doi.org/10.5194/amt-12-1337-2019.

Laucks, M.L., Davis, E.J., 1998. Chemical characterization of single pollen particles via fluorescence and Raman spectroscopy. J. Aerosol Sci. 29, 603–604. https://doi.org/10.1016/S0021-8502(98)00423-6.

Leontidou, K., Vernesi, C., De Groeve, J., Cristofolini, F., Vokou, D., Cristofori, A., 2018. DNA metabarcoding of airborne pollen: new protocols for improved taxonomic identification of environmental samples. Aerobiologia 34, 63–74. https://doi.org/10.1007/s10453-017-9497-z.

Leontidou, K., Vokou, D., Sandionigi, A., Bruno, A., Lazarina, M., De Groeve, J., et al., 2021. Plant biodiversity assessment through pollen DNA metabarcoding in natura 2000 habitats (Italian Alps). Sci. Rep. 11, 18226. https://doi.org/10.1038/s41598-021-97619-3.

Li, P., Flenley, J.R., 1999. Pollen texture identification using neural networks. Grana 38, 59–64. https://doi.org/10.1080/001731300750044717.

Longhi, S., Cristofori, A., Gatto, P., Cristofolini, F., Grando, M.S., Gottardini, E., 2009. Biomolecular identification of allergenic pollen: a new perspective for aerobiological monitoring? Ann. Allergy Asthma Immunol. 103 (6), 508–514. https://doi.org/10.1016/S1081-1206(10)60268-2 PMID: 20084845.

Matavulj, P., Brdar, S., Racković, M., Sikoparija, B., Athanasiadis, I.N., 2021. Domain adaptation with unlabeled data for model transferability between airborne particle identifiers. 17th International Conference on Machine Learning and Data Mining (MLDM 2021), New York, USA. https://doi.org/10.5281/zenodo.5574164.

Mitsumoto, K., Yabusaki, K., Kobayashi, K., Aoyagi, H., 2010. Development of a novel real-time pollen-sorting counter using species-specific pollen autofluorescence. Aerobiologia 26, 99–111. https://doi.org/10.1007/s10453-009-9147-1.

Molina, R.T., Maya-Manzano, J.M., Rodríguez, S.F., Garijo, A.G., Palacios, I.S., 2013. Influence of environmental factors on measurements with hirst spore traps. Grana 52, 59–70. https://doi.org/10.1080/00173134.2012.718359.

O'Connor, D.J., Healy, D.A., Hellebust, S., Buters, J.T.M., Sodeau, J.R., 2014. Using the WIBS-4 (Waveband integrated bioaerosol Sensor) technique for the on-line detection of pollen grains. Aerosol Sci. Technol. 48 (4), 341–349. https://doi.org/10.1080/02786826.2013.872768.

Oteros, J., Pusch, G., Weichenmeier, I., Heimann, U., Moller, R., Roseler, S., et al., 2015. Automatic and online pollen monitoring. Int. Arch. Allergy Immunol. 167, 158–166. https://doi.org/10.1159/000436968.

Oteros, J., Weber, A., Kutzora, S., Rojo, J., Heinze, S., Herr, C., 2020. An operational robotic pollen monitoring network based on automatic image recognition. Environ. Res. 191, 110031. https://doi.org/10.1016/j.envres.2020.110031 ISSN 0013-9351.

Pei, Z., Cao, Z., Long, M., Wang, J., 2018. Multi-adversarial domain adaptation. Thirty-Second AAAI Conference on Artificial Intelligence, New Orleans, Louisiana, USA. https://doi.org/10.48550/arXiv.1809.02176.

Pohlker, C., Huffman, J.A., Forster, J.-D., Poschl, U., 2013. Autofluorescence of atmospheric bioaerosols: spectral fingerprints and taxonomic trends of pollen. Atmos. Meas. Tech. 6 (12), 3369–3392. https://doi.org/10.5194/amt-6-3369-2013.

Polling, M., Sin, M., de Weger, L.A., Speksnijder, A.G.C.J., Koender, M.J.F., de Boer, H., Gravendeel, B., 2022. DNA metabarcoding using nrITS2 provides highly qualitative and quantitative results for airborne pollen monitoring. Sci. Total Environ. 806 (1), 150468. https://doi.org/10.1016/j.scitotenv.2021.150468.

Plaza, M.P., Kolek, F., Leier-Wirtz, V., Brunner, J.O., Traidl-Hoffmann, C., Damialis, A., 2022. Detecting airborne pollen using an automatic, real-time monitoring system: evidence from two sites. Int. J. Environ. Res. Public Health 19, 2471. https://doi.org/10.3390/ijerph19042471.

Robinson, E.S., Gao, R.-S., Schwarz, J.P., Fahey, D.W., Perring, A.E., 2017. Fluorescence calibration method for single-particle aerosol fluorescence instruments. Atmos. Meas. Tech. 10 (5), 1755–1768. https://doi.org/10.5194/amt-10-1755-2017.

Sakurai, T., Yonekura, S., Iinuma, T., Sakurai, D., Morimoto, Y., Kaneko, S., Okamoto, Y., 2018. The relationship of pollen dispersal with allergy symptoms and immunotherapy: allergen immunotherapy improves symptoms in the late period of japanese cedar pollen dispersal. Int. Arch. Allergy Immunol. 177, 245–254. https://doi.org/10.1159/000490314.

Sauliene, I., Sukiene, L., Daunys, G., Valiulis, G., Vaitkevicius, L., Matavulj, P., 2019. Automatic pollen recognition with the Rapid-E particle counter: the first-level procedure, experience and next steps. Atmos. Meas. Tech. 12 (6), 3435–3452. https://doi.org/10.5194/amt-12-1-2019.

Sauvageat, E., Zeder, Y., Auderset, K., Calpini, B., Clot, B., Crouzy, B., et al., 2020. Real-time pollen monitoring using digital holography. Atmos. Meas. Tech. 13 (3), 1539–1550. https://doi.org/10.5194/amt-13-1539-2020.

Scheifinger, H., Belmonte, J., Celenk, S., Damialis, A., Dechamp, C., Garcia-Mozo, H., 2013. Monitoring, modelling and forecasting of the pollen season. In: Sofiev, M., Bergmann, K.C. (Eds.), Allergenic Pollen. Springer, Dordrecht, pp. 71–126. https://doi.org/10.1007/978-94-007-4881-1_4.

Sikoparija, B., Mimic, G., Matavulj, P., Panic, M., Simovic, I., Brdar, S., 2019. Short communication: do we need continuous sampling to capture variability of hourly pollen concentrations? Aerobiologia 36, 3–7. https://doi.org/10.1007/s10453-019-09575-1.

Smith, M., Matavulj, P., Mimić, G., Panić, M., Grewling, L., Sikoparija, B., 2022. Why should we care about high temporal resolution monitoring of bioaerosols in ambient air? Sci. Total Environ. 826, 154231. https://doi.org/10.1016/j.scitotenv.2022.154231 ISSN 0048-9697.

Sofiev, M., Belmonte, J., Gehrig, R., Izquierdo, R., Smith, M., Dahl, A., Siljamo, P., 2013. Airborne pollen transport. In: Sofiev, M., Bergmann, K.C. (Eds.), Allergenic Pollen. Springer, Dordrecht. https://doi.org/10.1007/978-94-007-4881-1_5 PMID: 20084845.

Sofiev, M., 2019. On possibilities of assimilation of near-real-time pollen data by atmospheric composition models. Aerobiologia 35 (3), 523–531. https://doi.org/10.1007/s10453-019-09583-1.

Tesendic, D., Boberic-Krsticev, D., Matavulj, P., Brdar, S., Panic, M., Minic, V., Sikoparija, B., 2020. RealForAll: real-time system for automatic detection of airborne pollen. Enterp. Inf. Syst. https://doi.org/10.1080/17517575.2020.1793391.

Tummon, F., Adamov, S., Clot, B., Crouzy, B., Gysel-Beer, M., Kawashima, S., et al., 2021. A first evaluation of multiple automatic pollen monitors run in parallel. Aerobiologia. https://doi.org/10.1007/s10453-021-09729-0.

Tzeng, E., Hoffman, J., Darrell, T., Saenko, K., 2015. Simultaneous deep transfer across domains and tasks. Proceedings of the IEEE International Conference on Computer Vision, pp. 4068–4076. https://doi.org/10.48550/arXiv.1510.02192.